Regional heat flow and subsurface temperature patterns at Elysium Planitia and Oxia Planum areas, Mars

Journal Item

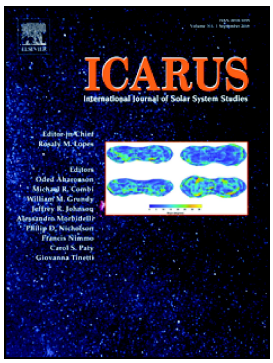

Regional heat flow and subsurface temperature patterns at Elysium Planitia and Oxia Planum areas, Mars

Isabel Egea-Gonzalez, Alberto Jiménez-Díaz, Laura M. Parro, Federico Mansilla, James A. Holmes, Stephen R. Lewis, Manish R. Patel, Javier Ruiz

PII: S0019-1035(19)30146-0
DOI: https://doi.org/10.1016/j.icarus.2019.07.013
Reference: YICAR 13379

To appear in: *Icarus*

Received date: 27 February 2019
Revised date: 14 June 2019
Accepted date: 12 July 2019

Please cite this article as: I. Egea-Gonzalez, A. Jiménez-Díaz, L.M. Parro, et al., Regional heat flow and subsurface temperature patterns at Elysium Planitia and Oxia Planum areas, Mars, Icarus, https://doi.org/10.1016/j.icarus.2019.07.013

Regional heat flow and subsurface temperature patterns at Elysium Planitia and Oxia Planum areas, Mars

Isabel Egea-Gonzalez [a,*], Alberto Jiménez-Díaz [b], Laura M. Parro [c], Federico Mansilla [c], James A. Holmes [d], Stephen R. Lewis [d], Manish R. Patel [d], Javier Ruiz [c]

[a] Departamento de Física Aplicada. Escuela Superior de Ingeniería, Universidad de Cádiz, 11519 Puerto Real, Cádiz, Spain

[b] Instituto de Ciencias de la Tierra Jaume Almera, ICTJA, CSIC, 08028 Barcelona, Spain

[c] Departamento de Geodinámica, Estratigrafía y Paleontología, Facultad de Ciencias Geológicas, Universidad Complutense de Madrid, 28040 Madrid, Spain

[d] School of Physical Sciences, The Open University, Milton Keynes, MK7 6AA, U.K.

* Corresponding author. E-mail: isabel.egea@uca.es (I. Egea-Gonzalez)

Abstract

Elysium Planitia and Oxia Planum are plains located near the Martian dichotomy. Lately, both regions have been extensively analyzed due to the major role that they play in the InSight and ExoMars missions. InSight landed in Elysium Planitia and will obtain the first direct measurement of surface heat flow on Mars. Similarly, the Rosalind Franklin rover on ExoMars 2020 will also provide useful information to understand the thermal state of the planet from data acquired in Oxia Planum, which is the preferred landing site. The proximity of the Martian dichotomy to the area surrounding both landing locations is an important source of spatial variability. In this work, we have modeled the heat flow and the subsurface temperature in the regions adjacent to both landing sites considering the regional context. In order to do so, we have solved the heat conduction equation by means of a finite element analysis and by taking into account topography, crustal composition, and crustal and megaregolith thicknesses. Our results indicate that the spatial variation in these parameters for the region surrounding the InSight landing site involves maximum differences in subsurface temperatures and surface heat flows between highlands and lowlands of about 67% and 16%, respectively. In regard to the area surrounding ExoMars landing site, these differences can reach 28% for subsurface temperatures, and 3% for surface heat flows. Crustal and megaregolith thicknesses together with the thermal properties of the megaregolith layer are the most influential factors affecting heat flows and temperature patterns. We also find that regional variations related to the dichotomy boundary are unlikely to have a large effect on the geothermal heat flux at the InSight and ExoMars landing sites.

Key words: Mars; Mars, surface; Thermal histories.

1. Introduction

Knowledge about surface heat flow is a key attribute to improve our understanding about the thermal evolution of a planet. Until now, estimates of the heat flows on the Martian surface have been calculated from indirect methods based on the depth of the brittle-ductile transition (e.g., Schultz and Watters, 2001; Grott et al., 2007; Ruiz et al., 2008, 2009), and on the flexure of the lithosphere under loads (e.g., Solomon and Head, 1990; McGovern et al., 2002, 2004; Grott et al., 2005; Phillips at al., 2008; Ruiz et al., 2006, 2011). These methods relate the mechanical strength and the thermal state of the lithosphere in order to determine the surface heat flow at the time when the lithosphere was faulted or loaded. The so-obtained results provide information about the thermal state of the planet in the past and serve as constraints for evolution models that analyze the thermal history of the planet (Ruiz et al, 2011; Ruiz, 2014). Other indirect methods consist in scaling the heat flow to Mars assuming chondritic composition (Fanale, 1976), and in establishing the heat flow that is compatible with basal melting of ice (Sori and Bramson, 2019).

Recently, the InSight mission has landed on Mars with the aim of obtaining the first direct measurement of the surface heat flow from the subsurface temperature and the regolith thermal conductivity. These data will be a major improvement in our knowledge about the present thermal state of Mars. The InSight landing site (4.5ºN, 135.6ºE) is located in the southwest of Elysium Planita, which is a broad plain in a volcanic province next to the Martian dichotomy (Golombek et al., 2018). Because the spacecraft does not move after landing, surface heat flow measurements will come from only this area. Previous works have described the characteristics of this region

thoroughly; the landing site is mapped as an Early Hesperian Transition Unit (Tanaka et al. 2014) covered by a smooth surface with low regional slope, a constant moderate albedo, and moderate THEMIS daytime IR signature (Golombek et al., 2017, 2018, 2019). The analysis of the regolith concluded that a layer of fine sand with low rock-abundance lies on the region as a result of impact gardening and eolian activity. This layer is thick enough to make possible the proper functioning of the heat flow probe that measures the temperature gradient in the subsurface (Golombek et al., 2017, 2018; Warner et al., 2017; Morgan et al., 2018). InSight will provide the surface heat flow in a single location, so a careful analysis of the effects of the regional context on the measured heat flow is necessary in order to interpret the data and constrain the planetary heat flow.

Parro et al. (2017) built a global model for the present-day surface heat flow by scaling the heat flow derived from the effective elastic thickness of the lithosphere beneath the North Polar Region (Phillips at al., 2008); the model took into account the radiogenic heat production, and variations in crustal thickness and topography. They obtained a result of 18 mW m^{-2} for the InSight landing site, and of 19 mW m^{-2} for the average planetary heat flow, and that therefore the local surface heat flow at this landing site would be roughly representative of the average value. Alternatively, Plesa et al. (2016a) estimated the difference between the global surface heat flow and the expected value at the landing site by using a 3-D thermal evolution model that included variations in crustal thickness and heat production. Their model predicts a strong correlation between the surface heat flow at the InSight landing site (18.8–24.2 mW m^{-2}) and the global value (23.2–27.3 mW m^{-2}).

However, global models might not be sufficient to estimate the surface heat flow on the area surrounding the InSight landing site. Previous works focused on the Apollo 15 and 17 sites have already shown that the regional context can influence greatly the thermal state of a studied area (e.g., Siegler and Smrekar, 2014 and references therein). Here we analyze how the regional features affect subsurface temperature and surface heat flows in the area that includes the southwest of Elysium Planita, the dichotomy and part of the nearby highlands. The dichotomy is the most prominent feature in the landscape of Mars. It divides the planet between the southern and northern hemisphere, and affects many aspects of the geology and geophysics of Mars (Watters et al., 2007). The origin of the dichotomy is not clear. Some hypotheses suggest an exogenic origin related with large impacts whereas other studies attempt to explain it through endogenic processes base on degree-1 mantle convection or plate tectonics (Watters et al., 2007; Andrews-Hanna et al., 2008). The dichotomy is an important source of spatial variability. Numerous studies have shown that the crustal properties vary greatly around the dichotomy boundary. Differences in topography and crustal thickness on either sides of the dichotomy near Elysium Planitia are significant and have been studied extensively (e.g., Milbury et al., 2007). Furthermore, the presence of felsic material in the southern hemisphere may imply a difference in crustal composition between the northern lowlands and the southern highlands (Baratoux, et al., 2014; Sautter et al., 2015), which could lead to a lateral variation of the crustal density across the dichotomy. Additionally, differences of the megaregolith thickness and of the thermal crustal properties are plausible.

On the other hand, Oxia Planum has been recommended as the landing site for the ExoMars 2020 mission. Oxia Planum is a Noachian plain located at 18ºN and 335ºE,

at the outlet of the Coogoon Valles system. This region is situated at the Martian dichotomy, in the transition between Arabia Terra, which is an extensively eroded area belonging to the highlands, and the northern Amazonian lowlands. Spectroscopic observations from OMEGA and CRISM instruments indicate that the region is covered by clay deposits rich in Mg/Fe phyllosilicates (Carter et al., 2016). Numerous pieces of evidence point to an important hydrological activity in Oxia Planum; various outflow channels crossed the area and fluvio-deltaic sediments are found on top of the clay-rich formation. A more recent layer formed by Amazonian lava flows lies over the deltaic sediments and the clay deposits, which are widely exposed at the landing site due to the ongoing erosion (Quantin et al., 2016).

In this work, we will study how the regional variability affects the heat flow pattern in the region around the InSight and ExoMars landing sites by means of a three-dimensional thermal conduction model that includes spatial variations of topography, crustal thickness, megaregolith thickness, and crustal thermal properties that are associated with the dichotomy boundary in these sites. Firstly, we will cinstruct three different models of growing complexity for the region including the InSight landing site. The first model (Model 1) takes into account the variation in crustal thickness and topography, the second model (Model 2) includes a megaregolith layer, and the third model (Model 3) considers different crustal compositions. Then, we apply the same method to obtain two different models (Models 4 and 5) of the region surrounding the ExoMars landing site. Model 4 is a three-layer model that includes mantle, crust and megaregolith, and Model 5 considers a change in the crustal composition. Our results allow us to evaluate the influence of regional features on the thermal state of these areas,

and give information about the subsurface temperatures and heat flow in the southwestern Elysium Planitia and around Oxia Planum.

2. Model approach

In order to study the influence of regional features on the thermal state around the InSight landing site, we have modeled a 1000 × 1100 km region in the southwestern Elysium Planitia. This zone includes the dichotomy and part of the southern highlands, which are the major features that can affect our results. **Figure 1a** shows the topography in the area surrounding the InSight landing site that is studied here (hereinafter referred to EP region), based on MOLA Mission Experiment Gridded Data Records (MEGDRs). The chosen area has been extended downwards to include the whole crust and at least 30 km of mantle. Our models assume heat conduction and a planar geometry. Thus, the size of the models is small enough to avoid melting and the spherical approach, but wide enough to allow lateral conduction in heat flow.

The Martian dichotomy crosses the EP region from northwest to southeast indicating the border between the southern highlands and the northern lowlands. The dichotomy boundary introduces an important spatial variability that could influence the thermal state of the EP region. The most obvious difference between lowlands and highlands is the contrast in elevation. It is expected that variations in topography that are small compared to the crustal thickness and the total depth of the model will have minor effects on our results about temperature and heat flow, but MOLA data (Smith et al., 2001) indicate that the maximum elevation difference between highlands and lowlands in the area surrounding InSight landing site is about 8 km, and the dichotomy scarp is 4 km high. In order to determine if this change between the two sides of the

dichotomy could be enough to influence the thermal state of the EP region, we have included topographic data with a horizontal resolution of 25 km per pixel in our models, which is enough to consider major differences in topography. Solving the heat equation with higher resolution would take into account small-scale topography, which will have no consequences in our results, but requires important computation resources. For the same reason, the geometry of the Gale crater has been simplified by increasing the average altitude of the crater bed by 800 m. This crater influences the local transport of heat, but it will have small effects at regional scale. An accurate model for this crater requires improving the vertical and horizontal resolution, and would complicate the regional model unnecessarily.

Together with a variation in altitude, the Martian dichotomy also represents a significant change in crustal thickness. Previous studies have shown that the crust thickens rapidly southwards across the dichotomy in the EP region such that the topography dichotomy matches well with the crustal thickness dichotomy (Zuber et al., 2000; Neumann et al., 2004). In order to include this thickness variation in our models, we have used the model obtained by Parro et al. (2017). These authors obtained a mean crustal thickness of, respectively, 40 km and 60 km under the lowlands and the highlands for the EP region. Furthermore, we have extended vertically our models to include a mantle thickness of at least 30 km. In this way, the mantle model is 30 km thick under the highlands, and 50 km under the lowlands for the EP region.

Megaregolith is a porous, fragmentary layer formed by large compact and coherent blocks with regolith material filling the gaps between them. This rubble has impact and ejecta origin, and covers the outer few meters–kilometers of a planet (e.g., Warren and Rasmussen, 1987; Ziethe et al., 2009). Megaregolith influences the thermal

state of a region because its thermal conductivity is much lower than that of equivalent solid rock. As a consequence, the megaregolith layer works as a blanket that insulates the hot interior and slows cooling down. The contrast between the smooth, scarcely cratered lowlands and the old heavily cratered highlands could involve a thicker megaregolith layer in this latter terrain. Although the Martian megaregolith thickness is not well constrained, we have considered a megaregolith of 2 km in the lowlands, which is a value generally assumed for Mars (Fanale, 1976; Zuber and Aist, 1990), and a somewhat thicker layer of 5 km in the highlands.

The megaregolith thermal conductivity is also uncertain and depends on multiple factors, such as porosity, temperature, composition, and filling materials in the gaps. There is some evidence about the thermal conductivity of the first few centimeters of the megaregolith, which consists of a fine dusty layer with an extremely low thermal conductivity. Based on brightness temperature observations, a value of 0.04 W m^{-1} K^{-1} has been proposed at the InSight landing site for the top centimeters of the surface (Putzig et al., 2005; Plesa et al., 2016b). However, the megaregolith thermal conductivity at depth is unclear. Lunar megaregolith conductivity is frequently assumed to be 0.2 W m^{-1} K^{-1} for a thickness of 2-3 km (Warren and Rasmussen, 1987; Haack et al., 1990; Zhang et al. 2013). This value may be too low for Mars because the presence of gas filling the gaps favors conduction, and the thicker megaregolith together with the higher gravity could contribute to narrow fractures. Furthermore, results in our models indicate that the thermal conductivity should be higher to avoid melting in the lower crust. Thus, we have considered a thermal conductivity of 0.8 W m^{-1} K^{-1} (see the Discussion section). Regarding the megaregolith density, we adopted an average value of 1700 kg m^{-3} following Plesa et al. (2016b).

Density and thermal conductivity in the crust depend on the assumed composition. Previous studies based on spectroscopic observations and on the analysis of SNC meteorites suggest a basaltic composition for the Martian crust (e.g., Mustard et al., 2005; Agee et al., 2013; Humayun et al., 2013). However, recent work points to the existence of a substantial amount of felsic rocks in the southern hemisphere (Carter and Poulet, 2013; Wray et al., 2013; Baratoux et al., 2014; Sautter et al., 2015). We have modeled both scenarios to study the effect of different compositions in the thermal state of the two studied areas. In the first instance, we have assumed a basaltic crust in our models with a crustal density of 2900 kg m^{-3} (e.g., Zuber et al., 2000; McGovern et al., 2002; Ruiz et al., 2008) and a thermal conductivity of 2 W m^{-1} K^{-1}(Beardsmore and Cull, 2001). Then, in a second scenario, we include a felsic composition in the highlands. In this case, we use a thermal conductivity of 2.5 W m^{-1} K^{-1} (Beardsmore and Cull, 2001), and a density of 2750 kg m^{-3}, which are more appropriate for felsic material (Fountain et al., 1990). Note this scenario is an extreme one, since that the martian crust is unlikely to be mostly felsic (Udry et al., 2018). We also assume steady state heat conduction, so it is not necessary to define the specific heat of each modeled layer. For modeling the mantle, we have assumed a density of 3500 kg m^{-3} and a thermal conductivity of 3.5 W m^{-1} K^{-1}, which are values widely used for the Martian mantle (e.g., Ruiz et al., 2008).

Radioactive heat production plays a major role in subsurface temperatures and surface heat flows. Data obtained by the Mars Odyssey GRS instrument allow to estimate the heat production at the surface of the planet from the abundance of K and Th measured in the first few centimeters of soil. Hahn et al. (2011) obtained small differences in the distribution of heat sources at the Martian surface, and provided an average heat production of 4.9 x 10^{-11} W kg^{-1}. We have adopted this value as

representative of the whole crust because the absence of large-scale crustal recycling together with the heavy cratering should have contributed to mix and homogenize the uppermost crust (Frey, 2006; Taylor et al., 2006). Previous studies suggest that the crust could be stratified such that the heat sources are concentrated in a layer thinner than the whole crust (Ruiz et al. 2009; Egea-González, 2017). However, the lack of information about the distribution of heat sources with depth prevents us from including a well founded variation of heat-producing elements (HPEs) into the crust.

In addition, the mantle heat generation is also included in our models. Internal heat generation in the studied areas comes mainly from the crust because HPEs are incompatible elements that concentrate in this layer. Nevertheless, radioactive heat production in the mantle could also contribute to the surface heat flow and influence the subsurface temperatures. Although the distribution of HPEs between the crust and mantle is uncertain, we have adopted a crustal enrichment factor of 10 (Hauck et al., 2002; Schumacher and Breuer, 2006; Grott and Breuer, 2009, Taylor and McLennan, 2009).

We solve the three dimensional heat conduction equation by means of a finite element analysis performed in the SimScale cloud-based platform (https://www.simscale.com/docs/). SimScale is based on open source codes and allows to carry out complex simulations without large computer resources. The geometry of the two studied areas is meshed with tetrahedral elements that are thinner near the surface. As boundary conditions, surface temperature and heat flow on the base of each model are defined. Surface temperatures were taken from the OpenMars database, a data repository for martian climate date based on assimilation of spacecraft observations into a Global Climate Model of Mars (Data are publicly accessible:

doi.org/10.21954/ou.rd.c.4278950.v1). For the EP region, annual-average surface temperatures vary in the range of 209–222 K depending on latitude and longitude (Holmes et al., 2015, 2017). However, this interval of temperature is small and does not influence our results. We use annual-average temperatures because the diurnal and annual thermal skin depths are very small compared to the model domain. While surface temperature is relatively well constrained, heat flow from the planetary interior is uncertain. For this magnitude, we have adopted a constant value of 10 mW m^{-2} obtained from the average present surface heat flow in Parro et al. (2017) at the EP region. For the four lateral sides of the models, we consider an infinite plane and assume a null heat flow along them.

For the study of the thermal state of the region surrounding the ExoMars landing site (hereinafter referred to OP region) we have followed the same procedure used for the EP region. **Figure 1b** shows the MEGDR topography for the OP region. We have calculated the surface heat flow and subsurface temperature around Oxia Planum by modeling an area of 1000 × 1000 km that includes the dichotomy. The model described in Parro et al. (2017) indicates that the crustal thickness is quite uniform under the OP region. Thus, we assume a thickness of 37 km, which is the average value provided by the model.

With respect to changes in topography, MOLA data reveal several channels and valleys that cross Oxia Planum and imply elevation contrasts of 1-2 km. The topographic dichotomy is not a scarp wall, but a softer regional slope from ESE to WNW, which involves a contrast in elevation of about 2 km. In order to study the influence of these topographic variations in our results, we have included topographic data with a horizontal resolution of 20 km per pixel for the OP region.

We use as boundary conditions for the OP region a null heat flow along the four lateral sides of the models, and a heat flow coming from the planetary interior of 13 mW m^{-2}. This value is derived from the average surface heat flow in Parro et al. (2017). As observed in the OpenMars database (doi.org/10.21954/ou.rd.c.4278950.v1), surface temperatures varies very little with latitude and longitude in this area, so we have assumed as boundary condition an average value of 221 K (Holmes et al., 2015, 2017).

Although the dichotomy boundary crosses the OP region, crustal thickness and topography are quite uniform. Unlike the Elysium Planitia case, there is not a well defined border separating two clearly different terrains in the OP region. Arabia Terra is defined as a highland terrain, but the crustal thickness in this area is more consistent with the lowlands. Therefore, we have considered two different options; firstly, we assume uniform properties for the entire region typical of the lowlands. This first model keeps a conductive mantle with a thickness of 30 km, a basaltic crust, and a megaregolith layer 2 km thick. These layers are characterized by the same density, thermal conductivity and heat production defined previously for the lowlands. Then, in a second model, we include different crustal composition and a different megaregolith thickness for lowlands and highlands. In this second option, our model supposes a 30 km thick mantle, a basaltic crust in the lowlands with a megaregolith layer of 2 km, and a felsic crustal composition in the highlands with a 5 km thick megaregolith. The properties of each layer are described above for the EP region.

Once we have solved the steady state heat conduction equation for the different models, we present an analysis of the results obtained for the vertical heat flow, the subsurface temperature, and the lateral heat flow from the highlands to the lowlands.

3. Results

We have studied how regional features affect the subsurface temperature and the surface heat flow patterns in the EP region by comparing results obtained from three increasingly complex models (Model 1, Model 2 and Model 3). **Table 1** and **2** summarize the properties and the main features in each model. The simplest model (Model 1) only takes into account differences in topography and crustal thickness. It considered a homogeneous basaltic crust at both sides of the dichotomy and does not include a megaregolith layer (**Figure 2a**). This model allows us to study how topographic and crustal thickness variations influence our results. Model 1 gives higher surface heat flows in the highlands because the internal heat generation is greater in the area with thicker crust (**Figure 3a**). Our results indicate that the average vertical heat flow is about 16% higher at the highland surface. This enhanced surface heat flow and the small temperature variation at the surface also lead to higher subsurface temperatures in the highlands. **Figure 3b** represents the subsurface temperature in a section of the studied area that goes from southwest to northeast. Temperatures rise quickly in the highlands reaching higher values under the region with thicker crust, where the insulating effect of the crust adds to the higher heat generation. The maximum temperature at the base of this model is 808 K. Lateral heat flow is small in the model, and it is only noticeable in very particular areas, like the base of the dichotomy, around deep craters, and in moderate elevations. The maximum horizontal heat flow is 2.8 mW m^{-2} and takes place in the mantle layer. Medium-scale topography causes horizontal heat flow because the preferred paths to evacuate heat divert towards lowers areas. In addition, heat also escapes through the slopes of the elevations. As a consequence, surface heat flow diminishes in elevations, and rises in lower areas.

However, this effect is small; variations in vertical heat flow between crater beds and rims are lower than 2 mW m^{-2} for craters in the highland regions. **Figure 3c** shows the horizontal heat flow from the highlands towards the north. The transference of heat is higher in the conductive mantle under the dichotomy due to the variation in the crustal thickness. The average heat flow towards the lowlands in the mantle is 0.4 mW m^{-2}. This lateral transport of heat involves a slight increase of vertical heat flow at the base of the dichotomy that can be noticed in Figure 3a. Nevertheless, the influence of lateral heat flow in our results is minor and confined to small areas. This model indicates that topographic and crustal variations by themselves do not influence the thermal state and heat flow of the InSight landing-site, which is about 15-16 mW m^{-2}.

Model 2 incorporates a megaregolith layer of variable thickness into Model 1, but keeps the basaltic crustal composition. Our results (**Figure 4a** and **4b**) show the same pattern obtained previously that gives higher surface heat flows and subsurface temperatures in the highlands. The average vertical heat flow is about 13% higher in the highlands. This value is lower than the obtained in Model 1 because the lower density and the lower thermal conductivity in the megaregolith diminish the surface heat flow at the highlands. The lower conductivity of the megaregolith layer increases notably the subsurface temperatures with respect to Model 1, which reaches 930 K under the highlands. Furthermore, the thicker megaregolith layer in the highlands favors the transference of heat towards the lowlands resulting in a lateral heat flow that is higher and goes further than in Model 1 (**Figure 4c**). In Model 2, the maximum lateral heat flow towards the north is 3.6 mW m^{-2}. Because heat is piped away from the highlands into the lowlands, the vertical heat flow diminishes slightly above the dichotomy scarp and grows at the base of the dichotomy in comparison with Model 1. The average

vertical heat flow at the base of the dichotomy scarp is about a 4% higher in relation to the average value for the rest of the lowlands.

The megaregolith thickness in Model 2 has been established from average altitude in the lowlands and the highlands: Thus, areas above (under) the average altitude have a thicker (thinner) megaregolth layer. This variability in the megaregolith thickness promotes horizontal heat flow and it is responsible of the small ups and downs of the vertical heat flow in the lowlands. However, as in the previous model, lateral heat flow in Model 2 is a local phenomenon and has little impact on our results at the InSight landing site.

Model 3 incorporates a felsic crustal composition in the highlands in contrast with Model 2. This variation in composition diminishes the differences on surface heat flow between the lowlands and the highlands (**Figure 5a**). Results obtained in the lowlands are similar to those calculated in Model 2 because the parameters that define the region are the same in both models. In the highlands, the higher thermal conductivity of the felsic rocks favors cooling, but its lower density diminishes the internal heat production resulting in lower surface heat flow than those calculated in Model 2. In Model 3, the average surface heat flow in the highlands is about 11% higher than the value obtained in the lowlands. This percentage is intermediate between Model 1 and 2. Minor heat generation and higher thermal conductivity also involve smaller lateral heat flow from the highlands to the north (**Figure 5c**), so surface heat flows in the lowlands next to the dichotomy are also a bit smaller in this model than in the previous one, as is noticeable in Figure 5c. Furthermore, heat flow coming from the mantle and the crust is focused on the crustal composition boundary increasing greatly the heat flow at the base of the megaregolith. When the heat that flows through the

compositional boundary found the irregular, low-conducting megaregolith layer, it evacuates towards the surface through the more efficient paths increasing lateral heat flow in the area around the compositional contact. A more conducting crust also diminishes subsurface temperatures respecting to values obtained in Model 2 (**Figure 5b**). Supplementary Material includes vertical temperatures profiles to compare results obtained for each model at different locations. The crustal composition variation involves lower heat generation and higher thermal conductivity in the highlands. This combination compensates the insulating effect of the megaregolith and its thickness variation leading to intermediate results between those obtained in Model 1 and 2.

With respect to the OP region, we have analyzed the results obtained through two different models (Model 4 and 5). **Table 3** outlines the main features of both models. Our simplest model for this area (Model 4) considers uniform properties for the OP region. As has been mentioned before, Model 4 assumes a basaltic crust with a thickness of 37 km, a 2 km thick megaregolith layer and a conductive mantle of 30 km (**Figure 2b**). These layers are characterized by the thermal properties and the heat production described before for the EP region. Model 4 provides surface heat flows that are more uniform than those calculated Elysium Planitia due to the lack of severe spatial heterogeneities in the regional features. There is no difference in the average vertical heat flows between the highlands and the lowlands in Model 4. This value is about 18 mW m^{-2} for both areas (**Figure 6a**). The topographic dichotomy plays a minor role resulting in a westward heat flow that is almost negligible. The maximum lateral heat flow is of 1.6 mW m^{-2}. However, valleys are marked with a distinct enhanced vertical heat flow because the walls and the lower altitude represent more efficient paths to evacuate heat. In general, subsurface temperatures for highlands and lowlands increase

with depth in a similar way, as can be noticed in **Figure 6b**, although somewhat higher values are reached under the region with higher average altitude; at the base of Model 4, the maximum temperature (684 K) is reached under the highlands, while the minimum value (540 K) is found under the lowlands.

In order to take into account possible differences linked to the dichotomy, we also modeled the OP region by assuming a variation in the megaregolith thickness and in the crustal composition. Thus, Model 5 increases the complexity of Model 4 by including a felsic crustal composition and a megaregolith thickness of 5 km in the highlands. Compositional variation in Model 5 leads to lower surface heat flows in the highlands because the lower density of the felsic crust diminishes the internal heat generation (**Figure 7a**). The difference in average vertical heat flow between highlands and lowlands is about 3% when the felsic composition is included. Similarly to Model 4, lateral heat flow is minor, and its effects are only appreciable in valleys and in the compositional boundary. The vertical heat flow on the floor of Ares Vallis is about a 6% higher than in the raised surroundings. As was explained in Model 3, heat is focused in the contact between different compositions increasing the vertical heat flow that goes into the megaregolith. This layer is very flat above the contact, so the most efficient way to evacuate heat is in the vertical towards the surface. For this reason, vertical heat flow is enhanced locally indicating the border between different compositions (red band in Figure 7a). Subsurface temperatures are somewhat lower than those calculated in Model 4 because the lower density implies lower heat generation (**Figure 7b**). In addition, the thicker megaregolith at the highlands increases temperatures in relation to the lowlands. The maximum temperature in the highlands for Model 5 is 668 K, while the maximum temperature at the lowlands is 520 K.

4. Discussion

According to our results, variations in regional features influence surface heat flow and subsurface temperature patterns. This is more evident in the EP region, where major spatial heterogeneities lead to remarkable variations in both magnitudes. Results obtained for the EP region indicate that the internal heat production plays a major role determining heat flows and subsurface temperatures, and consequently, the crustal thickness and the density are also key factors because higher values involve higher heat generation. This is the reason why the southern highlands have higher values of vertical heat flow. Furthermore, heat escapes through the more efficient pathways. Thus, the low thermal conductivity of the layers above the conductive mantle favors lateral heat towards areas with thinner crust. Although this lateral heat flow contributes to an increase/decrease of vertical heat flow at the base/top of the dichotomy scarp, its value is low and does not modify heat flows near the landing site. The major increase in the vertical heat flow at the base of the dichotomy due to the effect of the horizontal transport of heat occurs in Model 2. In this model, the average vertical heat flow at the base of the dichotomy is about a 4% higher in relation to the average value for the rest of the lowlands. The influence of the horizontal heat flow decreases with the distance to the dichotomy scarp and ceases before reaching the landing site. Therefore, our results indicate that the variation in crustal thickness under the dichotomy will not affect the data provided by InSight.

Megaregolith is also important to establish heat flows and subsurface temperatures, but the properties of this layer are highly unconstrained. The insulating effect of the megaregolith increases subsurface temperatures greatly. The megaregolith

layer rises subsurface temperatures in Model 2 with respect to Model 1. Results obtained from these models provide maximum temperatures in the mantle of 930 K and 808 K for, respectively, Model 2 and Model 1. Information about the plausible thickness and thermal conductivity of the megaregolith layer can be obtained from the melting temperature of the crust. The current water abundance in the Martian crust is poorly known, and therefore we take into account wet and dry conditions to calculate the respective wet and dry solidus of basalts (see Yasuda et al., 1994; Ruiz, 2007; Vogt et al., 2012). The base of the crust under the southern highlands melts at about 980 K and 1380 K for, respectively, wet and dry crust. Modelled crustal temperatures must be lower than this value in order to avoid melting. Taking into account this restriction, we have carried out several tests to constrain the thermal conductivity of a 5 km thick megaregolith layer. Our results indicate that the thermal conductivity must be over 0.2 W m^{-1} K^{-1} to keep temperature above the wet solidus in the lower crust of the southern highlands. Based on these calculations, we assume a megaregolith thermal conductivity of 0.8 W m^{-1} K^{-1}. Temperatures at depth obtained with these parameters, and shown in Figure 4b, are nearly an upper limit; a thicker or more insulating megaregolith could lead to the melting of the crustal base in the wet case. Given that the thickness and thermal conductivity of the megaregolith layer are not well constrained, we have performed two additional models (see Supplementary Material) to show how different values of these parameters affects temperatures and heat flow.

In addition, Model 2 and 3 demonstrate that small variations in the megaregolith thickness influence the vertical heat flow at the local level. In our models, the megaregolith thickness is established from the average altitude in the lowlands and the highlands. Therefore, valleys and hills that are under/above the average altitudes have a

thinner/thicker megaregolith. The thickness difference promotes lateral heat flows because heat is driven through the more conductive way, which is the one with thinner megaregolith. This horizontal transport of heat is responsible for the rises and falls in vertical heat flows that are shown in Model 2 and 3. The influence of the variable thickness is local, but can be significant. Our results indicate that the differences in vertical heat flow between crater beds and the elevated surroundings can be as high as 20 mW m^{-2} in Model 3. These results agree with previous work that studied the influence at regional scale of the megaregolith thickness on vertical and lateral heat flows (e.g. Warren and Rasmussen, 1987). Based on our results, the megaregolith layer may have an effect on InSight and ExoMars landing sites. Megaregolith heterogeneities near the InSight landing site are plausible and must be analyzed in order to evaluate the megaregolith significance on the heat flow measurements.

Composition is a crucial factor determining heat flow and temperatures at depth. The felsic crustal composition diminishes the vertical and lateral heat flows in the highlands. Felsic rocks are characterized by a lower density and a higher thermal conductivity. The lower density diminishes internal heat production leading to lower vertical heat flows and subsurface temperatures. In addition, the higher conductivity of felsic rocks also contributes diminishing temperatures at depth. The felsic composition reduces the average vertical heat flow at the highlands in a value close to 3% in comparison with Model 2. Furthermore, the maximum temperature at the base on the Model 3 goes down to 834 K against the maximum value of 930 K obtained for Model 2. The cooler and more conductive crust also reduces the horizontal heat flow in the mantle, which is a 2% higher in Model 2. Results obtained from Model 3 indicate that the variation in composition compensates and softens the effects of other regional

heterogeneities. Recently, Goossens at al. (2017) suggest an average bulk crustal density of about 2600 kg m^{-3} by using the admittance between topography and imperfect gravity; this lower density, if confirmed by further work, would imply a lower crustal heat production, which in turn would lead to lower surface heat flows and a cooler crust.

At the border between felsic and basaltic compositions, variations in the heat flow are significant because heat concentrates in the felsic-basaltic contact before reaching the megaregolith. Then, depending on the thickness and shape of the megaregolith layer, heat escapes through different pathways affecting the local heat flow. Note that the sharp compositional boundaries in our models are improbable but useful to understand the modifications in the transport of heat due to compositional differences. The increase of heat in the border between different compositions has been studied before and a similar focusing effect has been described by Siegler and Smrekar (2014). These authors found a maximum in vertical heat flows near the Apollo Heat Flow Experiments sites due to the concentration of heat along the highlands/mare border. The InSight landing site is not affected by the felsic-basaltic boundary because its influence is spatially-limited. However, local compositional differences near the landing site may alter the heat flow pattern.

Our results also find that variations in topography have little impact on heat flows. Medium-size craters and moderate elevations make heat to flow laterally from elevated to depressed areas. Nevertheless, differences in surface heat flow due to topography are small and confined around the elevation contrast. Variation in vertical heat flow between the floor of craters and the elevated terrain around them in Model 1 allows to make an estimation of the effect of topography without the megaregolith

component. The uniform colors in Figure 3a indicate that the variation in surface heat flows due to topography is small: this variation is lower than 6 mW m^{-2} for craters in the highlands.

Data coming from InSight will be taken far enough from the dichotomy to not be affected by the spatial heterogeneities linked to the highlands/lowlands boundary. However, further information about variations in local megaregolith and thermal conductivity next to the landing site is necessary in order to determine their influence on the measured heat flows.

According to our models, the surface heat flow in the InSight place would be about 15–16 mW m^{-2}. Nevertheless, it is worth mentioning that surface heat flow is determined by internal heat generation and heat flow coming from the interior, which are both uncertain magnitudes. Thus, the aim of these models is not to find absolute values of surface heat flow, but understanding how regional heterogeneities affect the thermal state of the studied area.

The thinner crust in the OP region involves a lower crustal heat flow component. As a consequence, the subsurface temperatures are lower than those obtained for the EP region despite the higher heat flow coming from the interior. Maximum modeled temperature for the OP region is of 684 K. In addition, the OP region lacks large regional contrasts, so results are also more homogeneous. Even assuming a contrast in crustal composition and megaregolith thickness between lowlands and highlands, heat flow and temperatures are quite uniform; Model 5 gives a difference in average vertical heat flow between highlands and lowlands of about 3%. Relevant changes in heat flows are only present in valleys and in the compositional border. The vertical heat flow grows in valleys because the lower elevation of the floor and the thinner megaregolith

contribute to concentrate heat. The vertical heat flow on the floor of Ares Vallis is about a 6% higher than the raised surroundings. Furthermore, as has been already discussed, differences in composition concentrate heat and may cause variations in heat flow. As the Elysium Planitia case, surface heat flow at ExoMars place does not depend on the regional features, but layering and the variety of surface terrains in the studied area could imply local variations in megaregolith thickness and thermal conductivities. Therefore, a close examination of the local context is required in order to determine its influence on the ExoMars landing site.

5. Conclusions

In this work, we have modeled the areas surrounding InSight and ExoMars landing sites with the aim of evaluating the influence of the regional characteristics on the heat flows and subsurface temperatures. Our models include major variations in topography, crustal and megaregolith thicknesses, and crustal composition that are associated with the dichotomy boundary. The influence of these parameters modifies considerably heat flow and temperature patterns in the studied regions, in the vicinity where the contrasts take place (mainly around the dichotomy). However, these regional variations do not affect the thermal state at the landing sites. In the case of Elysium Planitia model, the influence of regional characteristics is lower than the uncertainty of the heat flow measurement, which is of ±5 mW m^{-2} (Spohn et al., 2018). Thus, the data that will be provided by InSight are not affected by the variables included in this study.

Our results indicate that internal heat production, megaregolith thickness, and differences in density and thermal conductivity play an important role determining heat flow and temperatures. Some evidence suggests that these parameters could vary near

the landing site; for instance, Golombeck et al. (2017) reported a regolith thickness variation between 1–17 m over Elysium Planitia, and also found changes in the thermal inertia. On the other hand, the region surrounding ExoMars site is formed by a considerable number of geological units and shows a complex history where erosion, transport and sedimentation are significant processes that can affect the properties of the materials (Molina et al. 2017 and references therein). These pieces of evidence could indicate that variations of the most influential parameters in the heat conduction are possible near the landing sites, and could modify the local transport of heat. Further information about these parameters will help us to understand how local features influence results derived from InSight and ExoMars missions.

Acknowledgements

This work has received funding from the European Union's Horizon 2020 Programme (H2020-Compet-08-2014) under grant agreement UPWARDS-633127. I.E.-G. has received funding from project PR2017-074 (Universidad de Cádiz); the work by A.J.-D. was supported by a Juan de la Cierva-Formación postdoctoral contract (ref. FJCI-2016-28878) from the Spanish Ministry of Science, Innovation and Universities; the work by L.M.P. was supported by a FPU grant (2014/04842) from the Spanish Ministry of Education; L.M.P. is a Graduate Fellow of the Madrid City Council (Spain) at the Residencia de Estudiantes, 2018-2019. M.R.P., S.R.L. and J.A.H. acknowledge additional funding under UK Space Agency grant ST/R001405/1. We are grateful to José María Gutiérrez for helpful comments. We thank Michael Sori and an anonymous reviewer for their suggestions.

References

Agee, C., Wilson, N., McCubbin, F., Ziegler, K., Polyak, V., Sharp, Z., et al., 2013. Unique meteorite from early Amazonian Mars: Water-rich basaltic breccia Northwest Africa 7034. *Science* **339**, 780–785. https://doi.org/10.1126/science.1228858

Andrews-Hanna, J. C., Zuber, M. T., & Banerdt, W. B. (2008). The Borealis basin and the origin of the martian crustal dichotomy. *Nature*, *453*(7199), 1212.

Baratoux, D., Samuel, H., Michaut, C., Toplis, M. J., Monnereau, M., Wieczorek, M., ... & Kurita, K. (2014). Petrological constraints on the density of the Martian crust. *Journal of Geophysical Research: Planets*, *119*(7), 1707-1727.

Beardsmore, G.R., Cull, J.P., 2001. Crustal Heat Flow: A Guide to Measurement and Modelling. Cambridge University Press, Cambridge, 324 pp.

Carter, J., Poulet, F., 2013. Ancient plutonic processes on Mars inferred from the detection of possible anorthositic terrains. Nat. Geosci. 6, 1008–1012.

Carter, J., Quantin, C., Thollot, P., Loizeau, D., Ody, A., & Lozach, L. (2016, March). Oxia planum: A clay-laden landing site proposed for the ExoMars rover mission: Aqueous mineralogy and alteration scenarios. In *Lunar and Planetary Science Conference* (Vol. 47, p. 2064).

Egea-Gonzalez, I., Jiménez-Díaz, A., Parro, L. M., López, V., Williams, J. P., & Ruiz, J. (2017). Thrust fault modeling and Late-Noachian lithospheric structure of the circum-Hellas region, Mars. *Icarus*, *288*, 53-68.

Fanale, F. P. (1976). Martian volatiles: Their degassing history and geochemical fate. *Icarus*, *28*(2), 179-202.

Fountain, D.M., Salisbury, M.H., Percival, J., 1990. Seismic structure of the continental crust based on rock velocity measurements from the Kapuskasing Uplift, J. Geophys. Res. 95(B2), 1167–1186, doi:10.1029/JB095iB02p01167.

Frey, H. V. Impact constraints on, and a chronology for, major events in early Mars history. *J. Geophys. Res.* **111,** E08S91, doi:10.1029/2005JE002449 (2006)

Golombek, M., Kipp, D., Warner, N., Daubar, I. J., Fergason, R., Kirk, R. L., ... & Campbell, B. A. (2017). Selection of the InSight landing site. *Space Science Reviews*, *211*(1-4), 5-95.

Golombek, M., Warner, N. H., Grant, J. et al. 2019. Geology of the InSight landing site: Initial observations. LPSC Abstracts, 2132, 1694.

Golombek, M., Grott, M., Kargl, G. et al. 2018. Geology and Physical Properties Investigations by the InSight Lander. Space Sci Rev 214:84. https://doi.org/10.1007/s11214-018-0512-7

Grott, M., & Breuer, D. (2009). Implications of large elastic thicknesses for the composition and current thermal state of Mars. *Icarus*, *201*(2), 540-548.

Haack, H., Rasmussen, K. L., & Warren, P. H. (1990). Effects of regolith/megaregolith insulation on the cooling histories of differentiated asteroids. *Journal of Geophysical Research: Solid Earth*, *95*(B4), 5111-5124.

Hahn, B. C., McLennan, S. M. & Klein, E. C. Martian surface heat production and crustal heat flow from Mars Odyssey Gamma-Ray spectrometry. *Geophys. Res. Lett.* **38,** L14203, doi: 10.1029/2011GL047435 (2011).

Hauck, S. A., & Phillips, R. J. (2002). Thermal and crustal evolution of Mars. *Journal of Geophysical Research: Planets*, *107*(E7), 6-1.

Holmes, J. A., Lewis, S. R., & Patel, M. R. (2015). Analysing the consistency of martian methane observations by investigation of global methane transport. *Icarus*, *257*, 23-32.

Holmes, J. A., Patel, M. R., & Lewis, S. R. (2017). The vertical transport of methane from different potential emission types on Mars. *Geophysical Research Letters*, *44*(16), 8611-8620.

Humayun, M., Nemchin, A., Zanda, B., Hewins, R. H., Grange, M., Kennedy, A., et al. (2013). Origin and age of the earliest Martian crust from meteorite NWA 7533. *Nature*, **503**, 513–517.

McGovern, P.J. et al., 2002. Localized gravity/topography admittance and correlation spectra on Mars: Implications for regional and global evolution. J. Geophys. Res. 107, 5136. doi:10.1029/2002JE001854.

Milbury, C. A., Smrekar, S. E., Raymond, C. A., & Schubert, G. (2007). Lithospheric structure in the eastern region of Mars' dichotomy boundary. *Planetary and Space Science*, *55*(3), 280-288.

Molina, A., López, I., Prieto-Ballesteros, O., Fernández-Remolar, D., de Pablo, M. Á., & Gómez, F. (2017). Coogoon Valles, western Arabia Terra: Hydrological evolution of a complex martian channel system. *Icarus*, *293*, 27-44.

Morgan, P., Grott, M., Knapmeyer-Endrun, B. et al., 2018. A Pre-Landing Assessment of Regolith Properties at the InSight Landing Site. Space Sci Rev 214: 104. https://doi.org/10.1007/s11214-018-0537-y

Mustard, J., Poulet, F., Gendrin, A., Bibring, J.-P., Langevin, Y., Gondet, B., et al. (2005). Olivine and pyroxene diversity in the crust of Mars. *Science*, **307**, 1594–1597.

Neumann, G. A., Zuber, M. T., Wieczorek, M. A., McGovern, P. J., Lemoine, F. G., & Smith, D. E. (2004). Crustal structure of Mars from gravity and topography. *Journal of Geophysical Research: Planets*, *109*(E8).

Parro, L.M., Jiménez-Díaz, A., Ruiz, J., 2015. Current thermal state of Mars from scaled models of surface heat flow. EPSC Abstracts 10, EPSC2015-499.

Parro, L. M., Jiménez-Díaz, A., Mansilla, F., & Ruiz, J. (2017). Present-day heat flow model of Mars. *Scientific reports*, *7*, 45629.

Phillips, R. J., Zuber, M. T., Smrekar, S. E., Mellon, M. T., Head, J. W., Tanaka, K. L., ... & Safaeinili, A. (2008). Mars north polar deposits: Stratigraphy, age, and geodynamical response. *Science*, *320*(5880), 1182-1185.

Plesa, A. C., Grott, M., Tosi, N., Breuer, D., Spohn, T., & Wieczorek, M. A. (2016a). How large are present-day heat flux variations across the surface of Mars?. *Journal of Geophysical Research: Planets*, *121*(12), 2386-2403.

Plesa, A. C., Grott, M., Lemmon, M. T., Müller, N., Piqueux, S., Siegler, M. A., ... & Spohn, T. (2016b). Interannual perturbations of the Martian surface heat flow by atmospheric dust opacity variations. *Journal of Geophysical Research: Planets*, *121*(10), 2166-2175.

Putzig, N. E., Mellon, M. T., Kretke, K. A., & Arvidson, R. E. (2005). Global thermal inertia and surface properties of Mars from the MGS mapping mission. *Icarus*, *173*(2), 325-341.

Quantin, C., Carter, J., Thollot, P., Broyer, J., Lozach, L., Davis, J., ... & Allemand, P. (2016, March). Oxia Planum, the landing site for ExoMars 2018. In *47th Lunar and Planetary Science Conference Abstracts, Abstract* (Vol. 2863).

Ruiz, J., 2007. The heat flow during the formation of ribbon terrains on Venus. Planet. Space Sci. 55, 2063-2070.

Ruiz, J. et al., 2008. Ancient heat flow, crustal thickness, and lithospheric mantle rheology in the Amenthes region, Mars. Earth Planet. Sci. Lett. 270, 1–12.

Ruiz, J. *et al.* Ancient heat flows and crustal thickness at Warrego rise, Thaumasia Highlands, Mars: Implications for a stratified crust. *Icarus* **203,** 47–57 (2009).

Ruiz, J., McGovern, P. J., Jiménez-Díaz, A., López, V., Williams, J. P., Hahn, B. C., & Tejero, R. (2011). The thermal evolution of Mars as constrained by paleo-heat flows. *Icarus*, *215*(2), 508-517.

Ruiz, J. (2014). The early heat loss evolution of Mars and their implications for internal and environmental history. *Scientific reports*, *4*, 4338.

Sautter, V., Toplis, M. J., Wiens, R. C., Cousin, A., Fabre, C., Gasnault, O., ... & Bridges, J. C. (2015). In situ evidence for continental crust on early Mars. *Nature Geoscience*, *8*(8), 605.

Schumacher, S., & Breuer, D. (2006). Influence of a variable thermal conductivity on the thermochemical evolution of Mars. *Journal of Geophysical Research: Planets*, *111*(E2)

Siegler, M. A., & Smrekar, S. E. (2014). Lunar heat flow: Regional prospective of the Apollo landing sites. *Journal of Geophysical Research: Planets*, *119*(1), 47-63.

Smith, D. E., et al., (2001). Mars Orbiter Laser Altimeter: Experiment summary after the first year of global mapping of Mars. *Journal of Geophysical Research: Planets*, *106*(E10), 23689-23722.

Sori, M. M., & Bramson, A. M. (2019). Water on Mars, With a Grain of Salt: Local Heat Anomalies Are Required for Basal Melting of Ice at the South Pole Today. *Geophysical Research Letters*

Spohn, T., Grott, M., Smrekar, S. E., Knollenberg, J., Hudson, T. L., Krause, C., ... & Krömer, O. (2018). The heat flow and physical properties package (HP 3) for the InSight mission. *Space Science Reviews*, *214*(5), 96.

Tanaka, K. L., Robbins, S. J., Fortezzo, C. M., Skinner Jr, J. A., & Hare, T. M. (2014). The digital global geologic map of Mars: Chronostratigraphic ages, topographic and crater morphologic characteristics, and updated resurfacing history. *Planetary and Space Science*, *95*, 11-24.

Taylor, S.R., McLennan, S.M., 2009. Planetary crusts: Their composition, origin and evolution. Cambridge Univ. Press, Cambridge.

Taylor, G. J. *et al.* Variations in K/Th on Mars. *J. Geophys. Res.*, **111,** E03S06, doi: 10.1029/2006JE002676 (2006)

Vogt, K., Gerya, T.V., Castro, A., 2012. Crustal growth at active continental margins: Numerical modelling. Phys. Earth Planet. Int. 192–193, 1-20.

Udry, A., Gazel, E., & McSween Jr, H. Y. (2018). Formation of evolved rocks at Gale crater by crystal fractionation and implications for Mars crustal composition. *Journal of Geophysical Research: Planets*, *123*(6), 1525-1540.

Warner, N. H., Golombek, M. P., Sweeney, J., Fergason, R., Kirk, R., & Schwartz, C. (2017). Near surface stratigraphy and regolith production in southwestern Elysium Planitia, Mars: Implications for Hesperian-Amazonian terrains and the InSight lander mission. *Space Science Reviews*, *211*(1-4), 147-190.

Warren, P. H., & Rasmussen, K. L. (1987). Megaregolith insulation, internal temperatures, and bulk uranium content of the Moon. *Journal of Geophysical Research: Solid Earth*, *92*(B5), 3453-3465.

Watters, T. R., McGovern, P. J., & Irwin Iii, R. P. (2007). Hemispheres apart: The crustal dichotomy on Mars. *Annu. Rev. Earth Planet. Sci.*, *35*, 621-652.

Wray, J.J., et al., 2013. Prolonged magmatic activity on Mars inferred from the detection of felsic rocks. Nat. Geosci. 6, 1013–1017.

Yasuda, A., Fujii, T., Kurita, K., 1994. Meeting phase relations of an anhydrous mid-ocean ridge basalt from 3 to 20 GPa: implications for the behavior of subducted oceanic crust in the mantle. J. Geophys. Res. 99, 9401-9414.

Zhang, N., Parmentier, E. M., & Liang, Y. (2013). Effects of lunar cumulate mantle overturn and megaregolith on the expansion and contraction history of the Moon. *Geophysical Research Letters*, *40*(19), 5019-5023.

Zuber, M. T., & Aist, L. L. (1990). The shallow structure of the Martian lithosphere in the vicinity of the ridged plains. *Journal of Geophysical Research: Solid Earth*, *95*(B9), 14215-14230.

Zuber, M. T., Solomon, S. C., Phillips, R. J., Smith, D. E., Tyler, G. L., Aharonson, O., ... & Lemoine, F. G. (2000). Internal structure and early thermal evolution of Mars from Mars Global Surveyor topography and gravity. *science*, *287*(5459), 1788-1793.

	Conductivity (W m^{-1} K^{-1})	**Density (kg m^{-3})**
Mantle	3.5	3500
Basaltic crust	2	2900
Felsic crust	2.5	2750
Megaregolith	0.8	1700

Table 1. Properties of the different layers that compose the models.

		Layers	**Thickness (km)**
Model 1	Lowlands	Mantle	50
		Basaltic crust	40
	Highlands	Mantle	30
		Basaltic crust	60
Model 2	Lowlands	Mantle	50
		Basaltic crust	38
		Megaregolith	2
	Highlands	Mantle	30
		Basaltic crust	55
		Megaregolith	5
Model 3	Lowlands	Mantle	50
		Basaltic crust	38
		Megaregolith	2
	Highlands	Mantle	30
		Felsic crust	55
		Megaregolith	5

Table 2. Summary of the main features included in the models for the Elysium Planitia region.

		Layers	**Thickness (km)**

Model 4	Lowlands	Mantle	30
		Basaltic crust	35
		Megaregolith	2
	Highlands	Mantle	30
		Basaltic crust	35
		Megaregolith	2
Model 5	Lowlands	Mantle	30
		Basaltic crust	35
		Megaregolith	2
	Highlands	Mantle	30
		Felsic crust	32
		Megaregolith	5

Table 3. Summary of the main features included in the models for the Oxia Planum region.

Figure 1. MOLA digital elevation model in Equirectangular projection and 128 px/degree (MEGDR product) for the EP region **(a)** and for the OP region **(b)**. The black points indicate the landing sites. Elevations are above the aeroid.

Figure 2. **(a)** The simplest model used to study the thermal state around the InSight landing site (Model 1) together with a cross section view. This is a two-layer model where the crustal thickness varies between 40 km (lowlands) and 60 km (highlands). The gray block is the crust and the brown one is the mantle. The total depth of the model is 90 km and topographic data have a horizontal resolution of 25 km per pixel. This model assumes a basaltic crustal composition. **(b)** Model 4 geometry with a cross section view used to model the area around the ExoMars landing site**.** This model assumes a basaltic crust with a thickness of 37 km, a 2 km thick megaregolith layer and a conductive mantle of 30 km. The blue block represents the megaregolith.

Figure 3. **(a)** Vertical heat flow provided by Model 1 for the EP region. Lowlands and highlands show a remarkable contrast in vertical heat flow due to the difference in heat generation. The black dot represents the InSight landing site. The dashed lines indicate

the locations of the sections shown in (b) and (c). **(b)** Subsurface temperature in Model 1. The section goes from southwest to northeast. The highest temperatures are obtained under the highlands, where the crust is thicker. **(c)** Lateral heat flow from highlands (right) to lowlands (left) provided by Model 1 in the EP region. The lateral heat flow is more important under the dichotomy due to the variation in the crustal thickness. In order to improve the visualization, we have applied a vertical scale of 1.5.

Figure 4. **(a)** Vertical heat flow obtained through Model 2 for the EP region. Values at the base/top of the dichotomy are higher/lower than those calculated in Model 1. **(b)** Temperatures at depth for the diagonal dashed line in (a). The insulating effect of the megaregolith rises subsurface temperatures in comparison to Model 1. **(c)** Lateral heat flow from highlands (right) to lowlands (left) calculated from Model 2 for the vertical dashed line in (a). Megaregolith enhances the horizontal transport of heat towards the lowlands.

Figure 5. **(a)** Vertical heat flow provided by Model 3 for the EP region. Results are intermediate between models 1 and 2. The blue line is an effect of the composition

border and the megaregolith layer. **(b)** Model 3 results for subsurface temperatures in a SW-NE section corresponding to the diagonal dashed line in (a). The felsic composition cools the lithosphere relating to Model 2. **(c)** Lateral heat flow from highlands (right) to lowlands (left) calculated from Model 3. The horizontal transport of heat towards the lowlands diminishes in comparison to Model 2. The vertical line in (a) shows the section location.

Figure 6. (a) Vertical heat flow in the OP region obtained by Model 4. The model assumes a 30 km thick mantle, a basaltic crust with a thickness of 37 km, and a 2 km thick megaregolith layer. The thickness of each layer is established from the average altitude in the area. Heat is concentrated in valleys and craters due to the contrast in elevation and in the megaregolith thickness. The black dot is the preferred landing site for ExoMars. **(b)** Temperatures obtained at the OP region through Model 4 at the section indicated by the dashed line in (a). Temperatures increase at depth reaching higher values at the southeast of the studied region, where the heat production is somewhat higher.

Figure 7. (a) Vertical heat flow in the area surrounding ExoMars landing site (black dot) provided by Model 5. Crustal composition favors higher values in the lowlands. Heat is concentrated in valleys, deep craters, and in the compositional border. **(b)** Subsurface temperatures in Model 5 for a NS section of the studied area (dashed line). Highlands (right) are cooler than in the previous model due to the lower heat generation. Even though, temperatures at the highlands are higher than in the lowlands (left) due to the effect of a thicker megaregolith.

Highlights

We calculate heat flows and temperature patterns at Oxia Planum and Elysium Planitia

We solve the heat equation on each area by taking into account spatial variability

Our results show the influence of regional features on the thermal state of the areas

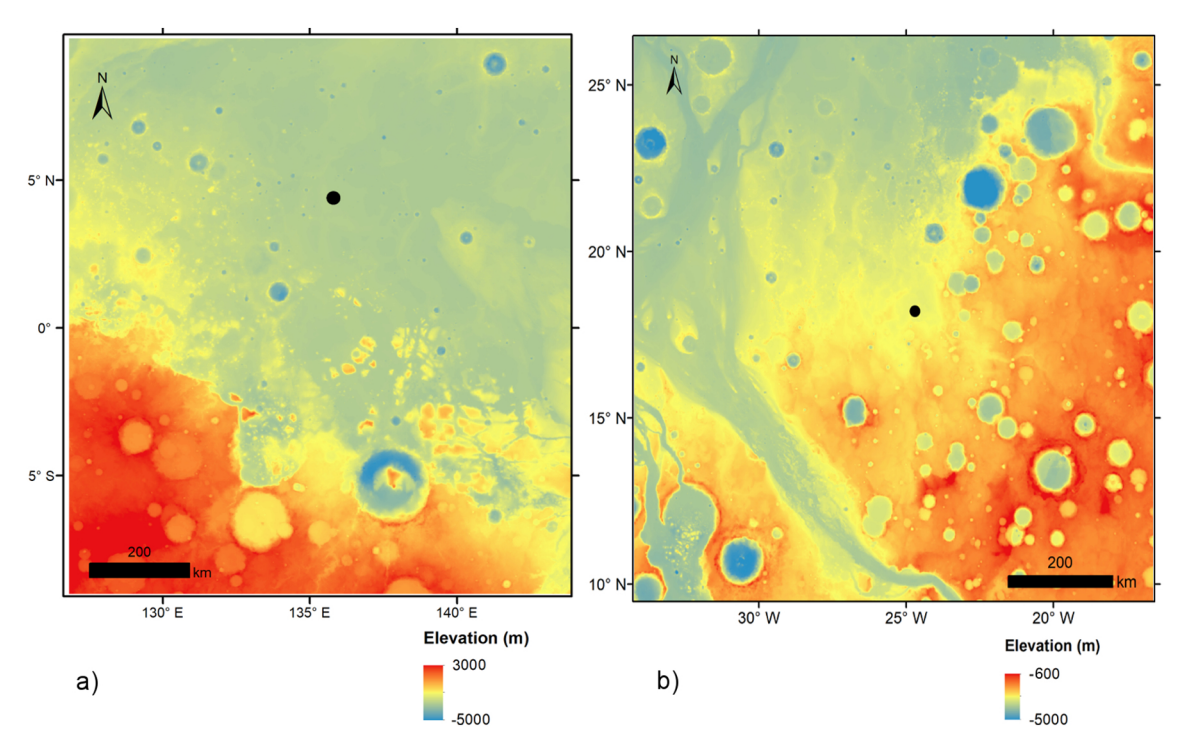
N
5° N
0°
5° S
200
km
130° E
135° E
140° E
Elevation (m)
3000
-5000
a)
N
25° N
20° N
15° N
10° N
200
km
30° W
25° W
20° W
Elevation (m)
-600
-5000
b)

Figure 1

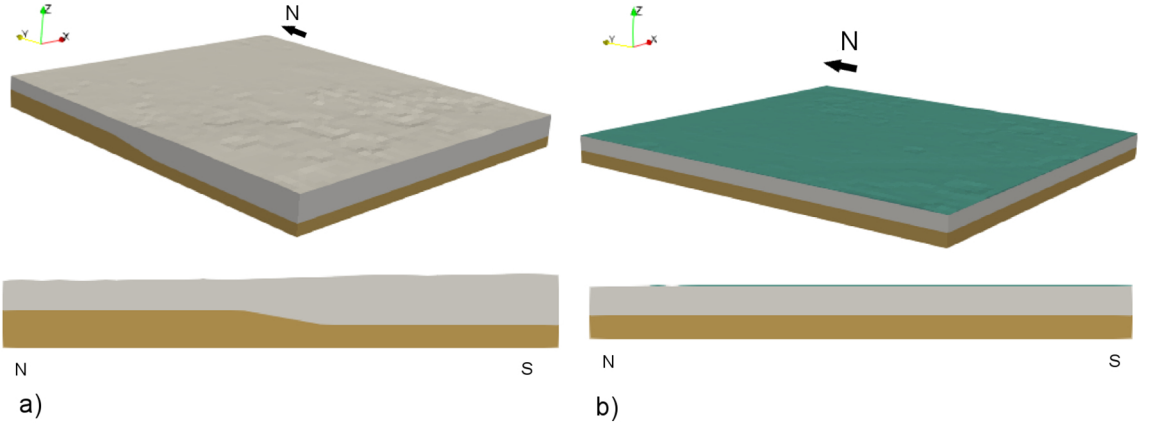

Figure 2

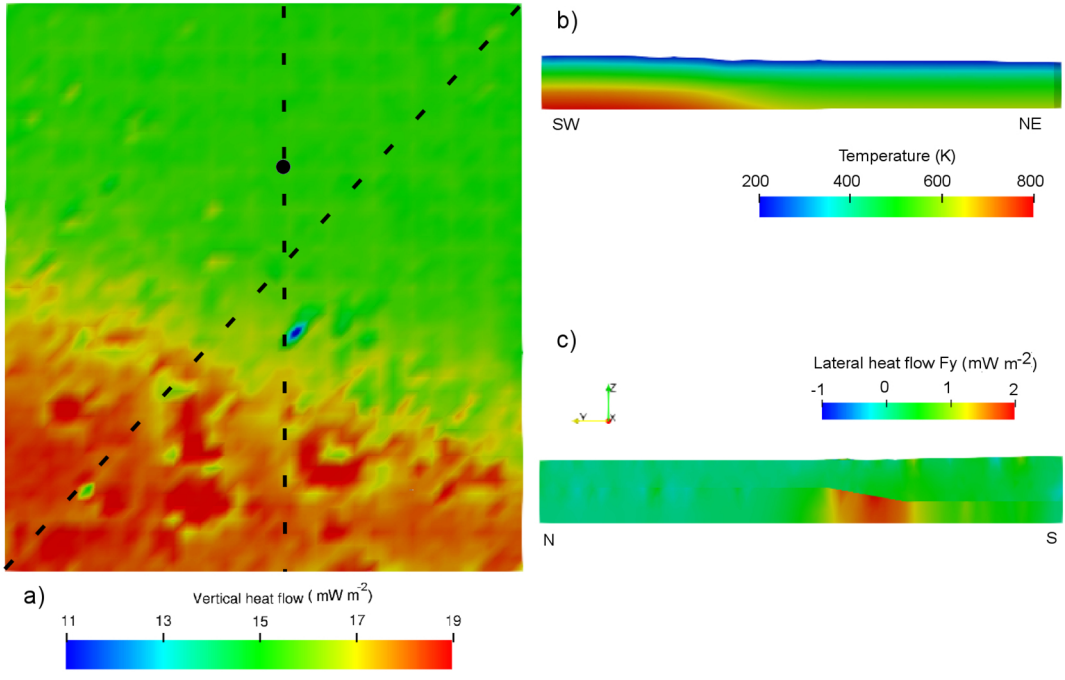
b)
SW
NE
Temperature (K)
200
400
600
800
c)
Lateral heat flow Fy (mW m-2)
-1
0
1
2
N
S
a)
Vertical heat flow (mW m-2)
11
13
15
17
19

Figure 3

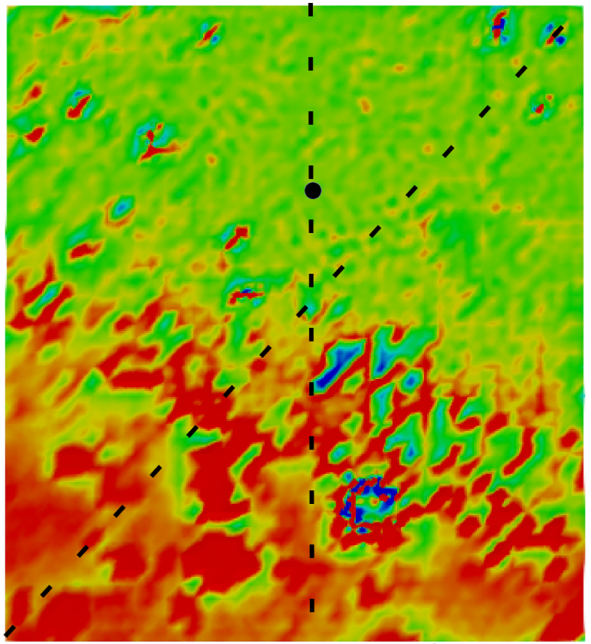

a)

Vertical heat flow (mW m^{-2})

11 13 15 17 19

b)

SW NE

Temperature (K)

350 550 750 950

c)

Lateral heat flow Fy (mW m^{-2})

-1 0 1 2

N S

Figure 4

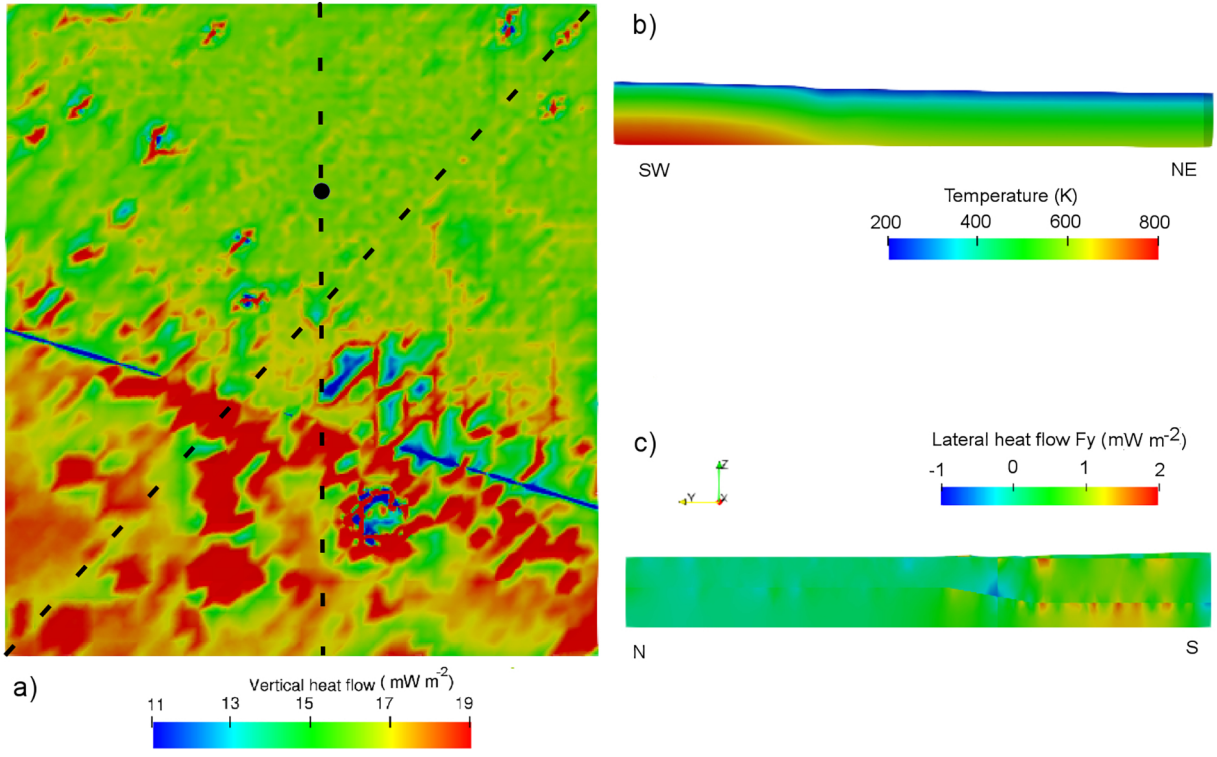
a)
Vertical heat flow (mW m-2)
11
13
15
17
19
b)
SW
NE
Temperature (K)
200
400
600
800
c)
Lateral heat flow Fy (mW m-2)
-1
0
1
2
N
S

Figure 5

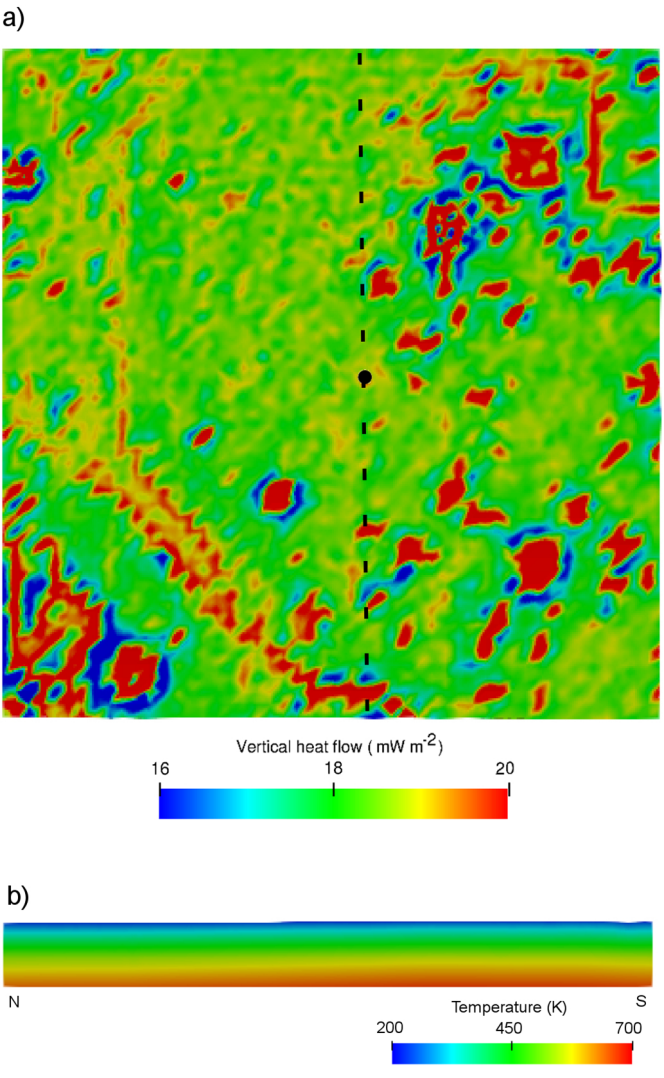
a)
Vertical heat flow (mW m-2)
16
18
20
b)
N
S
Temperature (K)
200
450
700

Figure 6

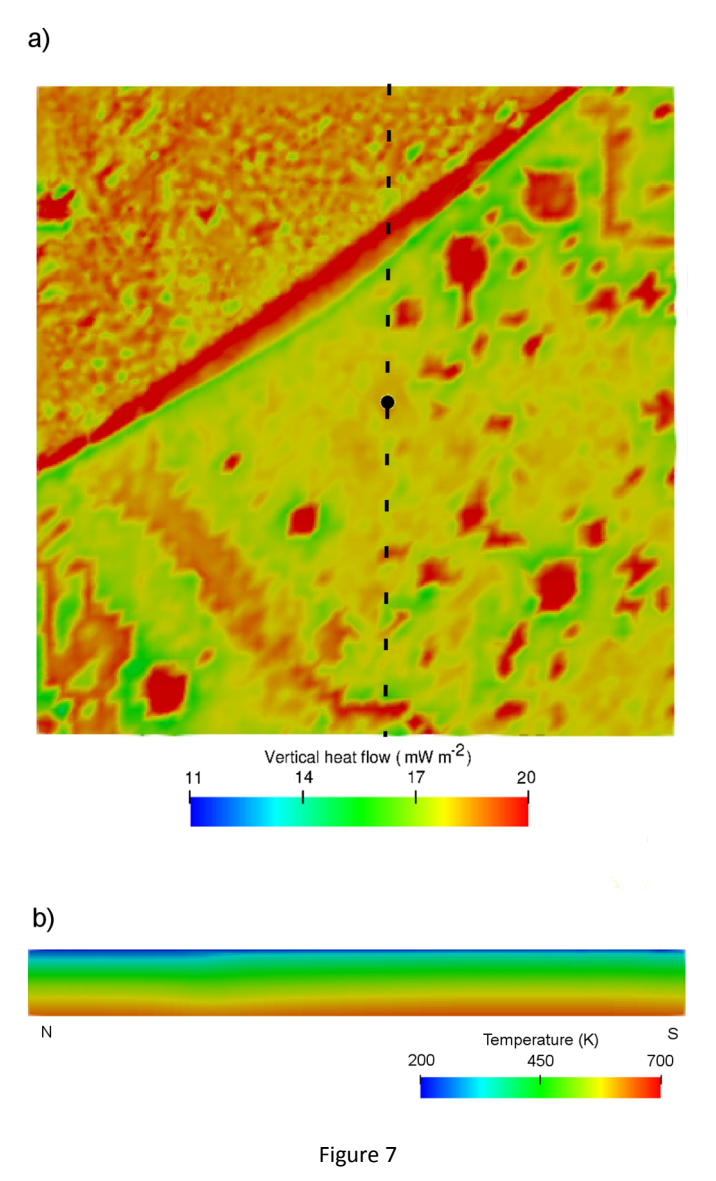
a)
Vertical heat flow (mW m-2)
11
14
17
20
b)
N
S
Temperature (K)
200
450
700

Figure 7

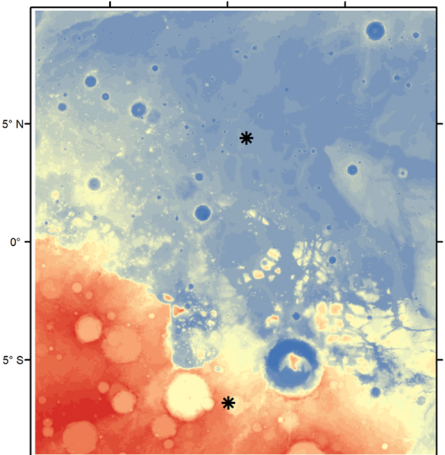
5° N
0°
5° S
130° E
135° E
140° E

a)

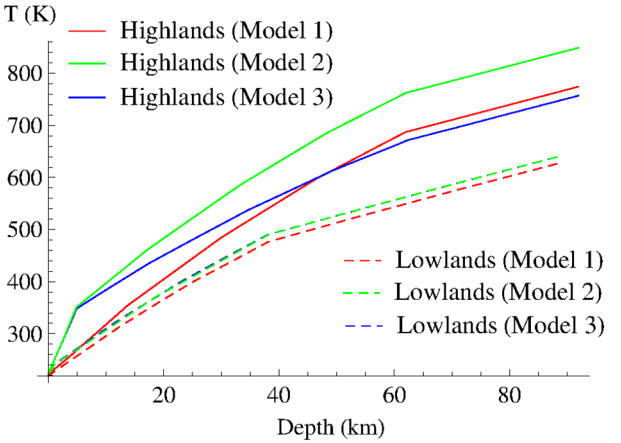
T (K)
Highlands (Model 1)
Highlands (Model 2)
Highlands (Model 3)
Lowlands (Model 1)
Lowlands (Model 2)
Lowlands (Model 3)
800
700
600
500
400
300
20
40
60
80
Depth (km)

b)

Figure 8

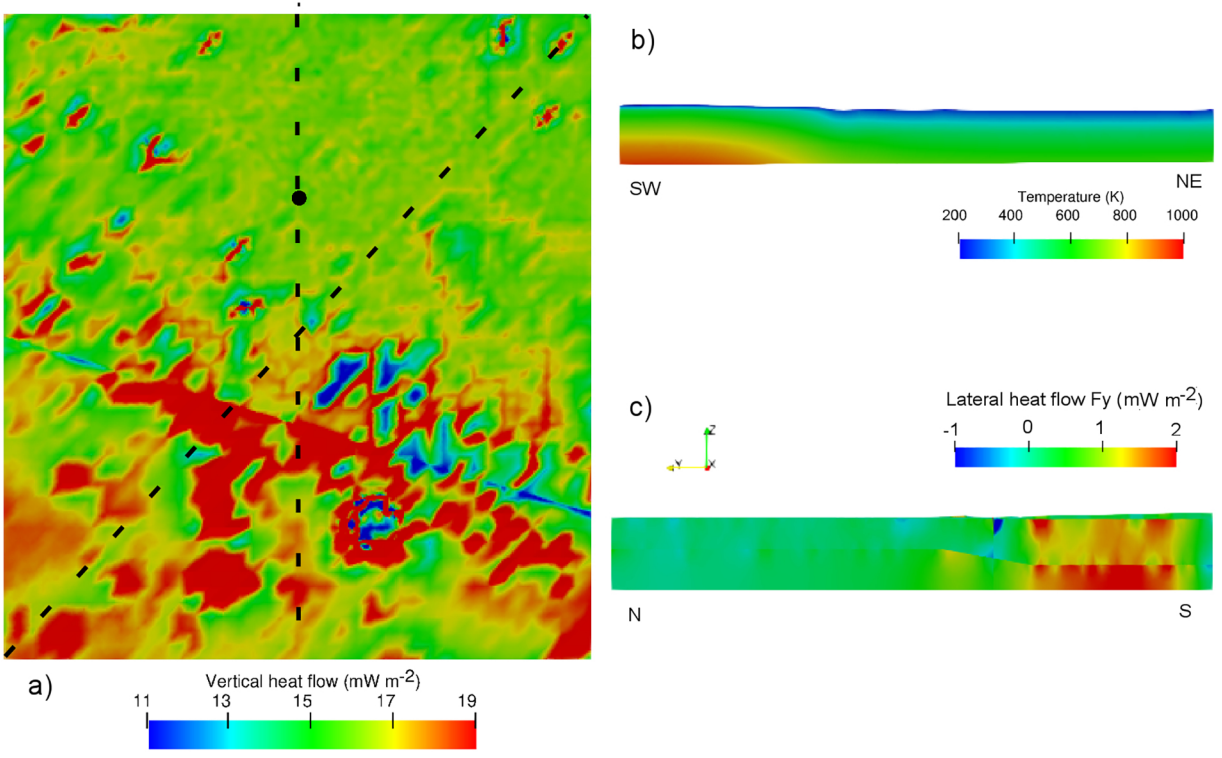
a)
Vertical heat flow (mW m-2)
11
13
15
17
19
b)
SW
NE
Temperature (K)
200
400
600
800
1000
c)
Lateral heat flow Fy (mW m-2)
-1
0
1
2
N
S

Figure 9

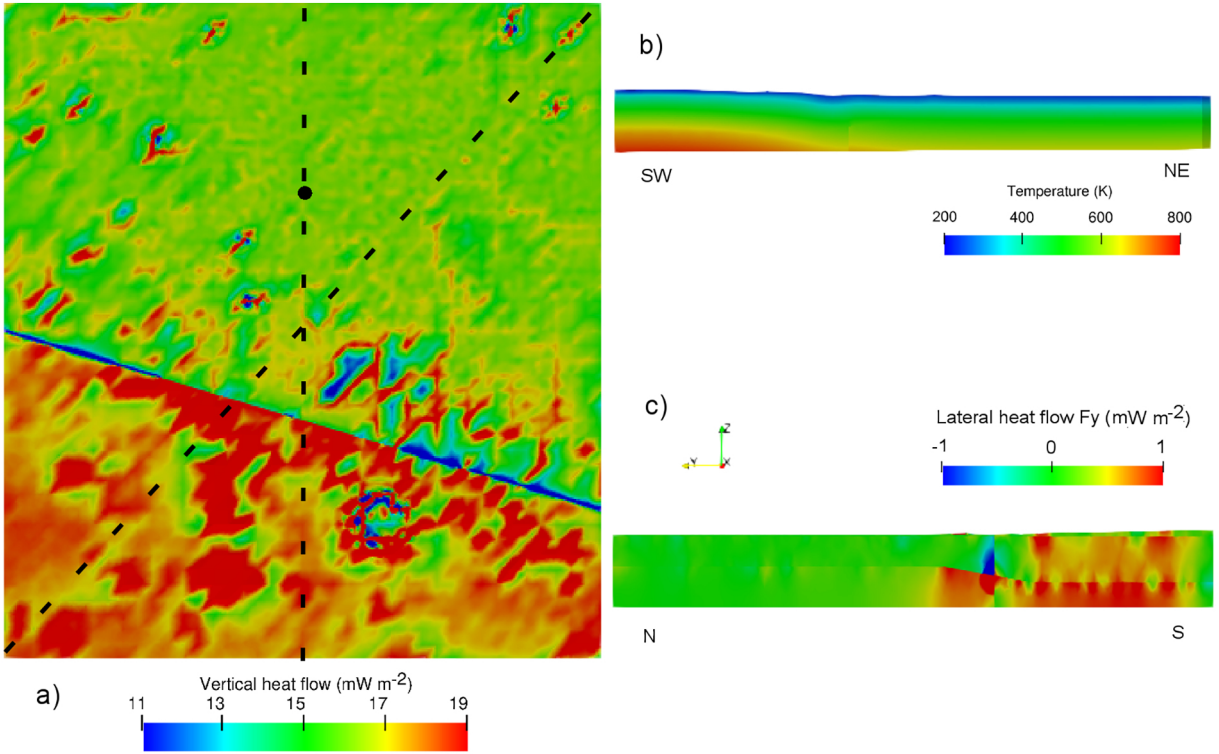
a)
Vertical heat flow (mW m-2)
11
13
15
17
19
b)
SW
NE
Temperature (K)
200
400
600
800
c)
Lateral heat flow Fy (mW m-2)
-1
0
1
N
S

Figure 10